Automatic Image Equalization and Contrast Enhancement Using Gaussian Mixture Modelling

Turgay Celik and Tardi Tjahjadi *Senior Member, IEEE*

Abstract

In this paper, we propose an adaptive image equalization algorithm which automatically enhances the contrast in an input image. The algorithm uses Gaussian mixture model (GMM) to model the image grey-level distribution, and the intersection points of the Gaussian components in the model are used to partition the dynamic range of the image into input grey-level intervals. The contrast equalized image is generated by transforming the pixels' grey levels in each input interval to the appropriate output grey-level interval according to the dominant Gaussian component and cumulative distribution function (CDF) of the input interval. To take account of human perception the Gaussian components with small variances are weighted with smaller values than the Gaussian components with larger variances, and the grey-level distribution is also used to weight the components in the mapping of the input interval to the output interval. Experimental results show that the proposed algorithm produces better or comparable enhanced images than several state-of-the-art algorithms. Unlike the other algorithms, the proposed algorithm is free of parameter setting for a given dynamic range of the enhanced image and can be applied to a wide range of image types.

Index Terms

Contrast enhancement, histogram equalization, normal distribution, Gaussian mixture modelling, histogram partition.

I. Introduction

The objective of an image enhancement technique is to bring out hidden image details, or to increase the contrast of an image with low dynamic range [1]. Such a technique produces an output image that subjectively looks better than the original image by increasing the grey level differences (*i.e.*, the contrast) among objects and background. Numerous enhancement techniques have been introduced and these can be divided into three groups: 1) techniques that decompose an image into high and low frequency signals for manipulation [2], [3]; 2) transform-based techniques [4]; and 3) histogram modification techniques [5]–[16].

Techniques in the first two groups often use multiscale analysis to decompose the image into different frequency bands and enhance its desired global and local frequencies [2]–[4]. These techniques are computationally complex but enable global and local contrast enhancement simultaneously by transforming the signals in the appropriate bands or scales. Furthermore they require appropriate parameter settings which might otherwise result in image degradations. For example, the centre-surround Retinex [2] algorithm was developed to attain lightness and colour constancy for machine vision applications. The constancy refers to the resilience of perceived colour and lightness to spatial and spectral illumination variations. The benefits of the Retinex algorithm include dynamic range compression and colour independence from the spatial distribution of the scene

This work was supported by the Warwick University Vice Chancellor Scholarship.

Turgay Celik and Tardi Tjahjadi are with the School of Engineering, University of Warwick, Gibbet Hill Road, Coventry, CV4 7AL, United Kingdom. e-mail: Turgay Celik (t.celik@warwick.ac.uk; celikturgay@gmail.com), Tardi Tjahjadi (t.tjahjadi@warwick.ac.uk).

illumination. However, this algorithm can result in “halo” artefacts, especially in boundaries between large uniform regions. Also, a “greying out” can occur, in which the scene tends to change to middle grey.

Among the three groups the third group received the most attention due to their straightforward and intuitive implementation qualities. Linear contrast stretching (LCS) and global histogram equalization (GHE) are two widely utilized methods for global image enhancement [1]. The former linearly adjusts the dynamic range of an image, and the latter uses an input-to-output mapping obtained from the cumulative distribution function (CDF) which is the integral of the image histogram. Since the contrast gain is proportional to the height of the histogram, grey levels with large pixel populations are expanded to a larger range of grey levels while other grey-level ranges with fewer pixels are compressed to smaller ranges. Although GHE can efficiently utilize display intensities, it tends to over-enhance the image contrast if there are high peaks in the histogram, often resulting in a harsh and noisy appearance of the output image. LCS and GHE are simple transformations but they do not always produce good results, especially for images with large spatial variation in contrast. In addition, GHE has the undesired effect of over-emphasizing any noise in an image.

In order to overcome the aforementioned problems, local histogram equalization (LHE) based enhancement techniques have been proposed, *e.g.*, [5], [6]. The LHE method [6] uses a small window that slides through every image pixel sequentially and only pixels within the current position of the window are histogram equalized, and the grey-level mapping for enhancement is done only for the centre pixel of the window. Thus, it utilises local information. However, LHE sometimes causes over-enhancement in some portion of the image and enhances any noise in the input image along with the image features. Furthermore, LHE based methods produce undesirable checkerboard effects.

Histogram Specification (HS) [1] is a method that uses a desired histogram to modify the expected output image histogram. However, specifying the output histogram is not a straightforward task as it varies from image to image. The Dynamic Histogram Specification (DHS) [7] generates the specified histogram dynamically from the input image. In order to retain the original histogram features, DHS extracts the differential information from the input histogram and incorporates extra parameters to control the enhancement such as the image original and the resultant gain control values. However, the degree of enhancement achievable is not significant.

Some researches have also focused on improving histogram equalization based contrast enhancement such as mean preserving bi-histogram equalization (BBHE) [8], equal area dualistic sub-image histogram equalization (DSIHE) [9] and minimum mean brightness error bi-histogram equalization (MMBEBHE) [10]. BBHE first divides the image histogram into two parts with the average grey level of the input image pixels as the separation intensity. The two histograms are then independently equalized. The method attempts to solve the brightness preservation problem. DSIHE uses entropy for histogram separation. MMBEBHE is the extension of BBHE that provides maximal brightness preservation. Although these methods can achieve good contrast enhancement, they also generate annoying side effects depending on the variation in the grey-level distribution [7]. Recursive Mean-Separate Histogram Equalization (RMSHE) [11] is another improvement of BBHE. However, it is also not free from side effects. Dynamic histogram equalization (DHE) [12] first smooths the input histogram by using a one dimensional smoothing filter. The smoothed histogram is partitioned into sub-histograms based on the local minima. Prior to equalizing the sub-histograms, each sub-histogram is mapped into a new dynamic range. The mapping is a function of the number of pixels in each sub-histogram, thus a sub-histogram with a larger number of pixels will occupy a bigger portion of the dynamic range. However, DHE does not place any constraint on maintaining the mean brightness of the image. Furthermore, several parameters are used that require appropriate setting for different images.

Optimisation techniques have also been employed for contrast enhancement. The method brightness preserving histogram

equalisation with maximum entropy (BPHEME) [13] defines the ideal histogram to have maximum entropy with brightness preservation. The target histogram which has the maximum differential entropy under the mean brightness constraint is obtained using variational approach [13]. BPHEME is designed to achieve maximum entropy. Although entropy maximisation corresponds to contrast stretching to some extent, it is not a straightforward consequence and does not definitely lead to contrast enhancement [14]. In flattest histogram specification with accurate brightness preservation (FHSABP) [14], convex optimisation is used to transform the image histogram into the flattest histogram, subject to a mean brightness constraint. An exact histogram specification method is used to preserve the image brightness. However, when the grey levels of the input image are equally distributed, FHSABP behaves very similar to GHE. Furthermore, it is designed to preserve the average brightness which may produce low contrast results when the average brightness is either too low or too high. In histogram modification framework (HMF) which is based on histogram equalization, contrast enhancement is treated as an optimization problem that minimizes a cost function [15]. Penalty terms are introduced in the optimisation in order to handle noise and black/white stretching. HMF can achieve different levels of contrast enhancement, through the use of different adaptive parameters. These parameters have to be manually tuned according to the image content to achieve high contrast. In order to design a parameter free contrast enhancement method, genetic algorithm (GA) is employed to find a target histogram which maximizes a contrast measure based on edge information [16]. We call this method contrast enhancement based on GA (CEBGA). CEBGA suffers from the drawbacks of GA based methods, namely dependency on initialization and convergence to a local optimum. Furthermore, the mapping to the target histogram is scored by only maximum contrast which is measured according to average edge strength estimated from the gradient information. Thus, CEBGA may produce results which are not spatially smooth. Finally, the convergence time is proportional to the number of distinct grey levels of the input image.

The aforementioned techniques may create problems when enhancing a sequence of images, or when the histogram has spikes, or when a natural looking enhanced image is required. In this paper, we propose an adaptive image equalization algorithm which is effective in terms of improving visual quality of different types of input images. Images with low-contrast are automatically improved in terms of an increase in dynamic range. Images with sufficiently high contrast are also improved but not as much. The algorithm further enhances the colour quality of the input images in terms of colour consistency, higher contrast between foreground and background objects, larger dynamic range and more details in image contents. The proposed algorithm is free from parameter setting. Instead the pixel values of an input image are modelled using Gaussian mixture model (GMM). The intersection points of the Gaussians in the model are used in partitioning the dynamic range of the input image into input grey-level intervals. The grey level of the pixels in each input interval are transformed according to the dominant Gaussian component and the CDF of the interval to obtain the contrast equalized image.

The paper is organized as follows. Section II presents the proposed automatic image equalization algorithm and the necessary background related to the GMM fit of the input image data. Section III presents the subjective and quantitative comparisons of the proposed method with several state-of-the-art enhancement techniques. Section IV concludes the paper.

II. Proposed Algorithm

Let us consider an input image, $\mathbf{X} = \{x(i,j) \mid 1 \leq i \leq H, 1 \leq j \leq W\}$, of size $H \times W$ pixels, where $x(i,j) \in \mathbb{R}$. Let us assume that $\mathbf{X}$ has a dynamic range of $[x_d, x_u]$ where $x(i,j) \in [x_d, x_u]$. The main objective of the proposed algorithm is to generate an enhanced image, $\mathbf{Y} = \{y(i,j) \mid 1 \leq i \leq H, 1 \leq j \leq W\}$, which has a better visual quality with respect to $\mathbf{X}$. The dynamic range of $\mathbf{Y}$ can be stretched or tightened into the interval $[y_d, y_u]$, where $y(i,j) \in [y_d, y_u]$, $y_d < y_u$ and $y_d, y_u \in \mathbb{R}$.

A. Modelling

The Gaussian mixture model (GMM) can model any data distribution in terms of a linear mixture of different Gaussian distributions with different parameters. Each of the Gaussian components has a different mean, standard deviation and proportion (or weight) in the mixture model. A Gaussian component with a low standard deviation and a large weight represents compact data with a dense distribution around the mean value of the component. When the standard deviation becomes larger, the data is dispersed about its mean value. The human eye is not sensitive to small variations around dense data, but is more sensitive to widely scattered fluctuations. Thus, in order to increase the contrast while retaining image details, dense data with low standard deviation should be dispersed while scattered data with high standard deviation should be compacted. This operation should be done so that the grey-level distribution is retained. In order to achieve this, we use GMM to partition the distribution of the input image into a mixture of different Gaussian components.

The grey-level distribution $p(x)$, where $x \in \mathbf{X}$, of the input image $\mathbf{X}$ can be modelled as a density function composed of a linear combination of N functions using the GMM [17], *i.e.*,

$$p(x) = \sum_{n=1}^{N} P(w_n)\, p(x|w_n), \tag{1}$$

where $p(x|w_n)$ is the nth component density, and $P(w_n)$ is the prior probability of the data points generated from component w_n of the mixture. The component density functions are constrained to be Gaussian distribution functions, *i.e.*,

$$p(x|w_n) = \frac{1}{\sqrt{2\pi\sigma_{w_n}^2}} \exp\left(-\frac{(x-\mu_{w_n})^2}{2\sigma_{w_n}^2}\right), \tag{2}$$

where μ_{w_n} and $\sigma_{w_n}^2$ are respectively the mean and the variance of the nth component. Each of the Gaussian distribution functions satisfies the constraint

$$\int_{-\infty}^{\infty} p(x|w_n)\, dx = 1, \tag{3}$$

and the prior probabilities are chosen to satisfy the constraints

$$\sum_{n=1}^{N} P(w_n) = 1 \quad \text{and} \quad 0 \leq P(w_n) \leq 1. \tag{4}$$

A GMM is completely specified by its parameters $\boldsymbol{\theta} = \left\{P(w_n), \mu_{w_n}, \sigma_{w_n}^2\right\}_{n=1}^{N}$. The estimation of the probability distribution function (PDF) of an input image data x reduces to finding the appropriate values of $\boldsymbol{\theta}$. In order to estimate $\boldsymbol{\theta}$, maximum likelihood estimation (MLE) techniques such as the expectation maximization (EM) algorithm [18] have been widely used. Assuming the data points $X = \{x_1, x_2, \ldots, x_{H\times W}\}$ are independent, the likelihood of the data X is computed by

$$\mathfrak{L}(X;\boldsymbol{\theta}) = \prod_{k=1}^{H\times W} p(x_k;\boldsymbol{\theta}) \tag{5}$$

given the distribution or, more specifically, given the distribution parameters $\boldsymbol{\theta}$. The goal of the estimation is to find $\hat{\boldsymbol{\theta}}$ that maximizes the likelihood, *i.e.*,

$$\hat{\boldsymbol{\theta}} = \underset{\boldsymbol{\theta}}{\operatorname{argmax}}\, \mathfrak{L}(X;\boldsymbol{\theta}). \tag{6}$$

Instead of maximizing this function directly, the log-likelihood $L(X;\boldsymbol{\theta}) = \ln \mathfrak{L}(X;\boldsymbol{\theta}) \equiv \sum_{k=1}^{H\times W} p(x_k;\boldsymbol{\theta})$ is used because it is analytically easier to handle.

The EM algorithm starts from an initial guess $\boldsymbol{\theta}^0$ for the distribution parameters and the log-likelihood is guaranteed to increase on each iteration until it converges. The convergence leads to a local or global maximum, but it can also lead to singular

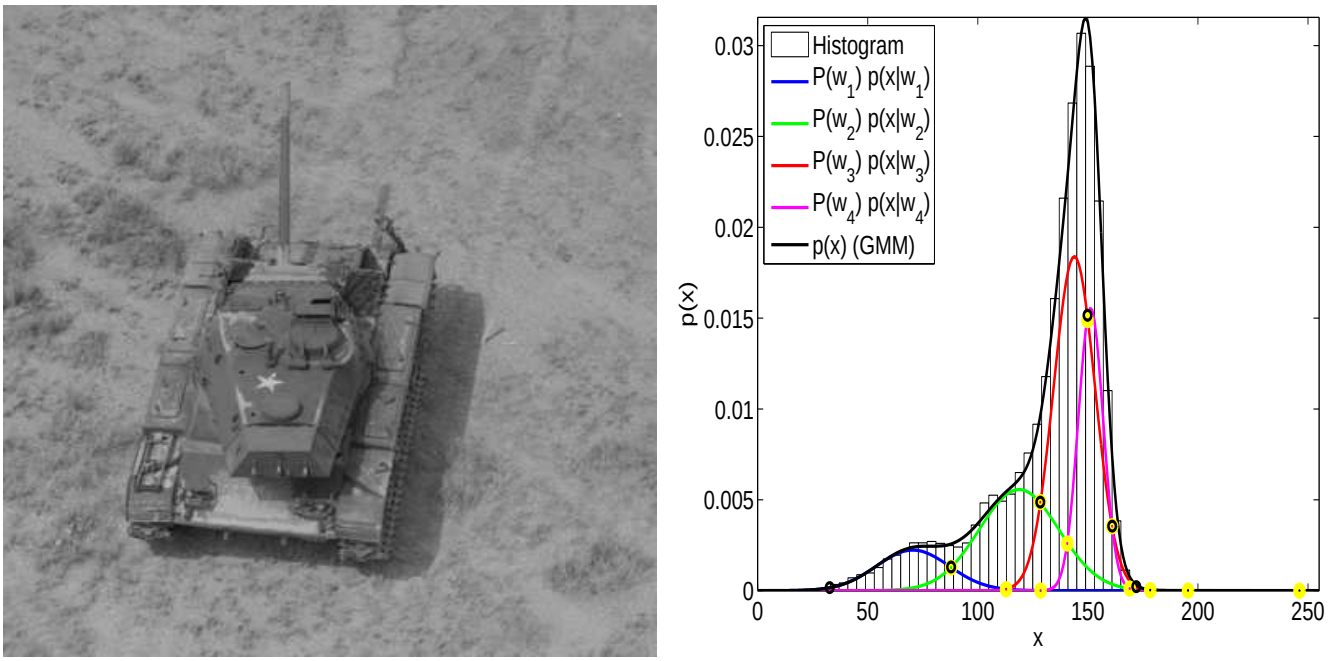

(a) (b)

Fig. 1. (a) A grey-level image; and (b) its histogram and GMM fit.

estimates, which is true particularly for Gaussian mixture distributions with arbitrary covariance matrices. The initialization is one of the problems of the EM algorithm. The selection of $\boldsymbol{\theta}^0$ (partly) determines where the algorithm converges or hits the boundary of the parameter space to produce singular, meaningless results. Furthermore, the EM algorithm requires the user to set the number of components, and the number is fixed during the estimation process.

The Figueiredo-Jain (FJ) algorithm [19] which is an improved variant of the EM algorithm overcomes major weaknesses of the basic EM algorithm. The FJ algorithm adjusts the number of components during estimation by annihilating components that are not supported by the data. It avoids the boundary when it annihilates components that are becoming singular. It is also allowed to start with an arbitrarily large number of components, which addresses the initialization of the EM algorithm. The initial guesses for component means can be distributed into the whole space occupied by the training samples, even setting one component for every single training sample. Due to its advantages over EM algorithm, in this work we adopt the FJ algorithm for parameter estimation.

Fig. 1(a) and (b) respectively illustrate an input image and its histogram together with its GMM fit. The histogram is modelled using four Gaussian components, *i.e.*, $N = 4$. The close match between the histogram (shown as rectangular vertical bars) and GMM fit (shown as solid black line) is obtained using FJ algorithm. There are three main grey tones in the input image corresponding to the tank, its shadow and the image background. The other grey-level tones are distributed around the three main tones. However, FJ algorithm results in four Gaussian components ($N = 4$) for the mixture model. This is because the grey tone with the highest average grey value corresponding to the image background has a deviation too large for a single Gaussian component to represent it. Thus it is represented by two Gaussian components, *i.e.*, w_3 and w_4 as shown in Fig. 1(b). All intersection points between Gaussian components that fall within the dynamic range of the input image are denoted by yellow circles, and significant intersection points that are used in dynamic range representation are denoted by black circles. There is only one dominant Gaussian component between two intersection points, which adequately represents the data within this grey-level interval. For instance, the range of the input data within the interval of $[35, 90]$ is represented by Gaussian

TABLE I

THE NUMERICAL VALUES OF INTERSECTION POINTS DENOTED BY YELLOW CIRCLES IN FIG. 1(B) BETWEEN COMPONENTS OF GMM FIT TO THE GREY-LEVEL IMAGE SHOWN IN FIG. 1(A).

	GMM Components			
	w_1	w_2	w_3	w_4
w_1	-	-718.88, 90.05	115.18, 225.52	129.46, 193.08
w_2	-718.88, 90.05	-	129.75, 172.39	141.31, 168.18
w_3	115.18, 225.52	129.75, 172.39	-	149.82, 163.54
w_4	129.46, 193.08	141.31, 168.18	149.82, 163.54	-

component w_1 (shown as solid blue line). Thus the data within each interval is represented by a single Gaussian component which is dominant with respect to the other components. The dynamic range of the input image is represented by the union of all intervals.

B. Partitioning

The significant intersection points are selected from all the possible intersections between the Gaussian components. The intersection points between two Gaussian components w_m and w_n are found by solving

$$P\left(w_m\right)p\left(x|w_m\right) = P\left(w_n\right)p\left(x|w_n\right), \tag{7}$$

or equivalently

$$-\frac{\left(x-\mu_{w_m}\right)^2}{2\sigma_{w_m}^2} + \frac{\left(x-\mu_{w_n}\right)^2}{2\sigma_{w_n}^2} = \ln\left(\frac{P\left(w_n\right)}{P\left(w_m\right)}\frac{\sigma_{w_m}}{\sigma_{w_n}}\right), \tag{8}$$

which results in

$$ax^2 + bx + c = 0, \tag{9}$$

where

$$a = \left(\sigma_{w_m}^2 - \sigma_{w_n}^2\right), \quad b = 2\left(\mu_{w_m}\sigma_{w_n}^2 - \mu_{w_n}\sigma_{w_m}^2\right),$$

$$c = \left(\mu_{w_n}^2\sigma_{w_m}^2 - \mu_{w_m}^2\sigma_{w_n}^2\right) - 2\sigma_{w_m}^2\sigma_{w_n}^2\ln\left(\frac{P\left(w_n\right)}{P\left(w_m\right)}\frac{\sigma_{w_m}}{\sigma_{w_n}}\right).$$

The second order parametric equation Eq. (9) has two roots, *i.e.*,

$$x_{m,n}^{(1)} = \frac{-b+\sqrt{b^2-4ac}}{2a}, \quad x_{m,n}^{(2)} = \frac{-b-\sqrt{b^2-4ac}}{2a}. \tag{10}$$

In Fig. 1(b) all intersection points between GMM components are denoted by yellow circles. The numerical values of the intersection points determined using Eq. (10) are shown in Table I. Table I is symmetric, *i.e.*, the intersection points between the components w_1 and w_2 are the same as the intersection points between components w_2 and w_1. The intersection points of two components are independent of the order of the components. All possible intersection points that are within the dynamic range of the image are detected. The leftmost intersection point between components w_1 and w_2 is at -718.88 which is not within the dynamic range of the input image, thus it could not be considered. In order to allow combination of intersection points to cover only the entire dynamic range of the input image a further process is needed.

The total number of intersection points calculated is $N(N-1)$. The significant intersection points $x_s^{(d)}$, where $d \in \{1,\ldots,D\}$, $D \leq N(N-1)$, are selected among all intersection points. For a given intersection point $x_{m,n}^{(k)}$, where $k=\{1,2\}$, between Gaussian components w_m and w_n it is selected as a significant intersection point if and only if it is a real number in the dynamic range of the input image, *i.e.*, $x_{m,n}^{(k)} \in \mathbf{X}$, and the Gaussian components w_m and w_n contain the maximum value in the mixture for the point $x_{m,n}^{(k)}$, *i.e.*,

$$P(w_m)\, p\left(x_{m,n}^{(k)}|w_m\right) = P(w_n)\, p\left(x_{m,n}^{(k)}|w_n\right), \tag{11}$$

$$P(w_m)\, p\left(x_{m,n}^{(k)}|w_m\right) > P(w_k)\, p\left(x_{m,n}^{(k)}|w_k\right), \tag{12}$$

where $\forall w_k \neq \{w_m, w_n\}$.

The significant intersection points are sorted in ascending order of their value and are partitioned into grey-level intervals to cover the entire dynamic range of $\mathbf{X}$, *i.e.*, $x \in x_s = \left[x_s^{(l)}, x_s^{(1)}\right] \cup \left[x_s^{(1)}, x_s^{(2)}\right] \cdots \cup \cdots \left[x_s^{(D)}, x_s^{(r)}\right]$. The leftmost significant intersection point $x_s^{(l)}$ is selected as the value of x for which

$$x_s^{(l)} = x, \quad F(x) \geq \frac{T_h}{HW}, \quad F(x-\Delta) < \frac{T_h}{HW}, \tag{13}$$

where the minimum distance between two consecutive numbers is Δ, *e.g.*, $\Delta = 1$ in the case of 8-bit input image $\mathbf{X}$ considered in this work, $F(x)$ is the CDF of x, and T_h is the minimum number of pixels which will be excluded from the tails of the grey-level distribution of x. To consider all pixel grey values of $\mathbf{X}$ we set $T_h = 1$. Similarly, the rightmost significant intersection point $x_s^{(r)}$ is selected by considering the tail of the grey-level distribution of x for which

$$x_s^{(r)} = x, \quad (1 - F(x)) \geq \frac{T_h}{HW}, \quad (1 - F(x+\Delta)) < \frac{T_h}{HW}. \tag{14}$$

The significant intersection points that fall outside of the interval $\left[x_s^{(l)}, x_s^{(r)}\right]$ are ignored since they are the intersection points between two Gaussian components that fall outside the dynamic range of $\mathbf{X}$, and x_s is updated as $x_s = \left[x_s^{(1)}, x_s^{(2)}, \ldots, x_s^{(K)}\right]$ with $x_s^{(1)} < x_s^{(2)} < \ldots < x_s^{(K)}$, where K is the maximum number of significant intersection points. In Fig. 1 the six significant intersection points are denoted by black circles, and the range of x_s covers the entire dynamic range of $\mathbf{X}$.

The CDF of x is

$$\begin{aligned} F(x) &= \int_{-\infty}^{x} p(x)\, dx = \int_{-\infty}^{x} \sum_{n=1}^{N} P(w_n)\, p(x|w_n)\, dx \\ &= \sum_{n=1}^{N} P(w_n) \int_{-\infty}^{x} \frac{1}{\sqrt{2\pi\sigma_{w_n}^2}} \exp -\frac{(x-\mu_{w_n})^2}{2\sigma_{w_n}^2} dx \\ &= \sum_{n=1}^{N} P(w_n) \int_{-\infty}^{\frac{(x-\mu_{w_n})}{\sqrt{2}\sigma_{w_n}}} \frac{1}{\sqrt{\pi}} \exp\left(-t^2\right) dt. \end{aligned} \tag{15}$$

It can be calculated using the closed form expression

$$F(x) = \sum_{n=1}^{N} P(w_n)\, F_{w_n}(x), \tag{16}$$

where $F_{w_n}(x)$ is the CDF of Gaussian component w_n, and using the definition of the error function ($\mathrm{erf}(x)$) (also called the Gauss error function) [20] it is computed as $F_{w_n}(x) = \beta\left(\frac{x-\mu_{w_n}}{\sqrt{2}\sigma_{w_n}}\right)$, where $\beta(x)$ is computed in terms of error function [20] as follows:

$$\beta(x) = \begin{cases} (1 + \mathrm{erf}(x))/2 & \text{, iff } x \geq 0 \\ \\ (1 - \mathrm{erf}(|x|))/2 & \text{, otherwise,} \end{cases} \tag{17}$$

where the numerical values of $\mathrm{erf}(x)$ are tabulated in [20]. The function $\beta(x)$ is invertible, *i.e.*, for a given $\beta(x) = a$, $x = \beta^{-1}(a)$ exists.

The consecutive pairs of significant intersection points are used to partition the dynamic range of $\mathbf{X}$ into subintervals, *i.e.*, $[x_d, x_u] = \left[x_s^{(1)}, x_s^{(2)}\right] \cup \left[x_s^{(2)}, x_s^{(3)}\right] \cup \cdots \cup \left[x_s^{(K-2)}, x_s^{(K-1)}\right] \cup \left[x_s^{(K-1)}, x_s^{(K)}\right]$. The subinterval $\left[x_s^{(k)}, x_s^{(k+1)}\right]$ is represented by a Gaussian component w_k which is dominant with respect to the other Gaussian components in the subinterval. The dominant Gaussian component is found by considering the a posteriori probability of each component in the interval $\left[x_s^{(k)}, x_s^{(k+1)}\right]$ which is equivalent to the area under the Gaussian component, *i.e.*,

$$w_k = \underset{\forall w_i}{\operatorname{argmax}} \left[F_{w_i}\left(x_s^{(k+1)}\right) - F_{w_i}\left(x_s^{(k)}\right)\right]. \tag{18}$$

C. Mapping

The interval $\left[x_s^{(k)}, x_s^{(k+1)}\right]$, where $k = 1, 2, \ldots, K-1$, in x_s is mapped onto the dynamic range of the output image $\mathbf{Y}$. In the mapping, each interval covers a certain range which is proportional to a weight α_k, where $\alpha_k \in [0, 1]$, which is calculated by considering two figure of merits simultaneously: 1) the rate of the total number of pixels that fall into the interval $\left[x_s^{(k)}, x_s^{(k+1)}\right]$; and 2) the standard deviation of the dominant Gaussian component w_k, *i.e.*,

$$\alpha_k = \frac{(\sigma_{w_k})^{\gamma}}{\sum_{i=1}^{N}(\sigma_{w_i})^{\gamma}} \; \frac{\left[F\left(x_s^{(k+1)}\right) - F\left(x_s^{(k)}\right)\right]}{\sum_{i=1}^{K-1}\left[F\left(x_s^{(i+1)}\right) - F\left(x_s^{(i)}\right)\right]}. \tag{19}$$

The first term adjusts the brightness of the equalized image, and $\gamma \in [0, 1]$ is brightness constant (in this paper $\gamma = 0.5$ is used). The lower the value of γ, the brighter is the output image. The second term in Eq. (19) is related to the grey-level distribution and is used to retain the overall content of the data in the interval. Eq. (19) maintains a balance between the data distribution and variance of the data in a certain interval. Since the human eye is more sensitive to sudden changes in widely scattered data and less sensitive to smooth changes in densely scattered data, Eq. (19) gives larger weights to widely scattered data (larger variance), and vice versa.

Using α_k, the input interval $\left[x_s^{(k)}, x_s^{(k+1)}\right]$ is mapped onto the output interval $\left[y^{(k)}, y^{(k+1)}\right]$ according to

$$\begin{aligned} y^{(k)} &= y_d + (y_u - y_d)\sum_{i=1}^{k-1}\alpha_i, \\ y^{(k+1)} &= y^{(k)} + \alpha_k (y_u - y_d). \end{aligned} \tag{20}$$

The above mapping guarantees that the output dynamic range is covered by the mapping, *i.e.*, $[y_d, y_u] = \left[y^{(1)} = y_d, y^{(2)}\right] \cup \left[y^{(2)}, y^{(3)}\right] \cup \cdots \cup \left[y^{(K-1)}, y^{(K)} = y_u\right]$.

In the final mapping of pixel values from the input interval onto the output interval, the CDF of the distribution in the output interval is preserved. Let Gaussian distribution $w_{k'}$ with parameters $\mu_{w_{k'}}$ and $\sigma^2_{w_{k'}}$ represent the Gaussian component w_k in the range $\left[y^{(k)}, y^{(k+1)}\right]$. The parameters $\mu_{w_{k'}}$ and $\sigma^2_{w_{k'}}$ are found by solving the following equations simultaneously

$$F_{w_k}\left(x_s^{(k)}\right) = F_{w_{k'}}\left(y^{(k)}\right), \tag{21}$$

$$F_{w_k}\left(x_s^{(k+1)}\right) = F_{w_{k'}}\left(y^{(k+1)}\right), \tag{22}$$

so that the area under the Gaussian distribution w_k between $\left[x_s^{(k)}, x_s^{(k+1)}\right]$ is equal to the area under the Gaussian distribution

$w_{k'}$ in the interval $\left[y^{(k)}, y^{(k+1)}\right]$. Using Eq. (17) together with equations Eq. (21) and Eq. (22), one can write

$$\beta\left(\frac{x_s^{(k)}-\mu_{w_k}}{\sqrt{2}\sigma_{w_k}}\right) = \beta\left(\frac{y^{(k)}-\mu_{w_{k'}}}{\sqrt{2}\sigma_{w_{k'}}}\right) \tag{23}$$

$$\beta\left(\frac{x_s^{(k+1)}-\mu_{w_k}}{\sqrt{2}\sigma_{w_k}}\right) = \beta\left(\frac{y^{(k+1)}-\mu_{w_{k'}}}{\sqrt{2}\sigma_{w_{k'}}}\right), \tag{24}$$

which is equivalent to

$$\frac{x_s^{(k)}-\mu_{w_k}}{\sqrt{2}\sigma_{w_k}} = \frac{y^{(k)}-\mu_{w_{k'}}}{\sqrt{2}\sigma_{w_{k'}}} \tag{25}$$

$$\frac{x_s^{(k+1)}-\mu_{w_k}}{\sqrt{2}\sigma_{w_k}} = \frac{y^{(k+1)}-\mu_{w_{k'}}}{\sqrt{2}\sigma_{w_{k'}}}. \tag{26}$$

Using equations Eq. (25) and Eq. (26), the parameters of Gaussian distribution $w_{k'}$ are computed as follows:

$$\mu_{w_{k'}} = \frac{\left(\frac{x_s^{(k)}-\mu_{w_k}}{x_s^{(k+1)}-\mu_{w_k}}y^{(k+1)} - y^{(k)}\right)}{\left(\frac{x_s^{(k)}-\mu_{w_k}}{x_s^{(k+1)}-\mu_{w_k}} - 1\right)} \tag{27}$$

$$\sigma_{w_{k'}} = \frac{\left(y^{(k)}-\mu_{w_{k'}}\right)}{\left(x_s^{(k)}-\mu_{w_k}\right)}\sigma_{w_k}. \tag{28}$$

The mapping of x to y, where $x \in \left[x_s^{(k)}, x_s^{(k+1)}\right]$ and $y \in \left[y^{(k)}, y^{(k+1)}\right]$, is achieved by keeping the CDFs of Gaussian distribution w_k and Gaussian distribution $w_{k'}$ equal, *i.e.*,

$$\beta\left(\frac{x-\mu_{w_k}}{\sqrt{2}\sigma_{w_k}}\right) - \beta\left(\frac{x_s^{(k)}-\mu_{w_k}}{\sqrt{2}\sigma_{w_k}}\right) = \beta\left(\frac{y-\mu_{w_{k'}}}{\sqrt{2}\sigma_{w_{k'}}}\right) - \beta\left(\frac{y^{(k)}-\mu_{w_{k'}}}{\sqrt{2}\sigma_{w_{k'}}}\right), \tag{29}$$

where using the equality in Eq. (23),

$$\beta\left(\frac{x-\mu_{w_k}}{\sqrt{2}\sigma_{w_k}}\right) = \beta\left(\frac{y-\mu_{w_{k'}}}{\sqrt{2}\sigma_{w_{k'}}}\right) \quad \Rightarrow \quad \frac{x-\mu_{w_k}}{\sqrt{2}\sigma_{w_k}} = \frac{y-\mu_{w_{k'}}}{\sqrt{2}\sigma_{w_{k'}}}$$

results in the following mapping of given x to the corresponding y according to the Gaussian distributions w_k and $w_{k'}$

$$y = \left(\frac{x-\mu_{w_k}}{\sigma_{w_k}}\right)\sigma_{w_{k'}} + \mu_{w_{k'}}. \tag{30}$$

The final mapping from x to y is achieved by considering all Gaussian components in the GMM to retain the pixel distributions in input and output intervals equal. Using the superposition of distributions together with Eq. (30) one can find

$$y = \sum_{i=1}^{N}\left(\left(\frac{x-\mu_{w_i}}{\sigma_{w_i}}\right)\sigma_{w_{i'}} + \mu_{w_{i'}}\right)P_{w_i}. \tag{31}$$

Fig. 2(a), (b) and (c) respectively show the input images, equalized images using the proposed algorithm where the dynamic range of the output image is $[y_d, y_u] = [0, 255]$, and the mappings between input image data points (x) and equalized output image data points (y) are according to Eq. (31). Fig. 2(c) shows that a different mapping is applied to a different input grey-level interval. Fig. 2(b) shows that the proposed algorithm increases the brightness of the input image while keeping the high contrast between object boundaries. The input image in the second row of Fig. 2(a) has only fifteen different grey levels, thus it is difficult to observe the image features. The proposed algorithm linearly transforms the grey levels as shown in Fig. 2(c) so that the image features are easily discernable in Fig. 2(b).

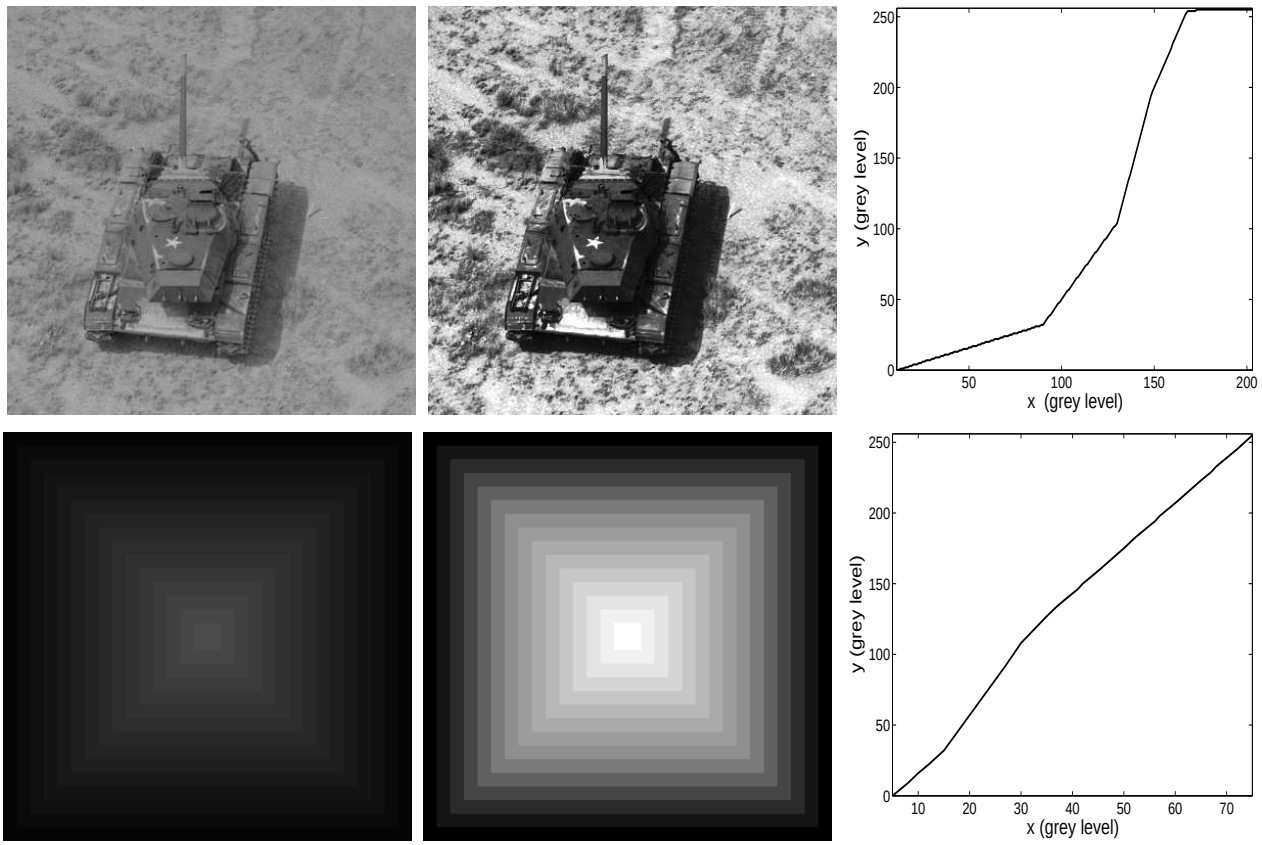

(a) (b) (c)

Fig. 2. (a) A grey-level input image $\mathbf{X}$; (b) The equalized output image $\mathbf{Y}$ using the proposed algorithm; and (c) The data mapping between the input and output images.

One approach to extend the grey-scale contrast enhancement to colour images is to apply the method to their luminance component only and preserve the chrominance components. Another is to multiply the chrominance values with the ratio of their input and output luminance values to preserve the hue. The former approach is employed in this paper where an input *RGB* image is transformed to CIE $L^*a^*b^*$ colour space [1] and the luminance component L^* is processed for contrast enhancement. The inverse transformation is then applied to obtain the contrast enhanced *RGB* image.

III. Experimental Results

A dataset comprising standard test images from [21]–[24] is used to evaluate and compare the proposed algorithm with our implementations of GHE [1], BPHEME [13], FHSABP [14], CEBGA [16] and the weighted histogram approximation of HMF [15]. GHE, BPHEME, FHSABP and CEBGA are free of parameter selection but HMF requires parameter tuning which is manually selected according the input test images. It is worth to note that for FHSABP method exact histogram specification is used [14] to achieve high degree of brightness preservation between input and output images. The test images show wide variations in terms of average image intensity and contrast. Thus they are suitable for measuring the strength of a contrast enhancement algorithm under different circumstances.

An output image is considered to have been enhanced over the input image if it enables the image details to be better perceived. An assessment of image enhancement is not an easy task as an improved perception is difficult to quantify. Nevertheless, in practice it is desirable to have both quantitative and subjective assessments. It is therefore necessary to establish a basis which

defines a good measure of enhancement. We use absolute mean brightness error (*AMBE*) [10], discrete entropy (*DE*) [25], and edge based contrast measure (*EBCM*) [26] as quantitative measures. For colour images, the contrast enhancement is quantified by computing these measures on their luminance channel L^* only.

AMBE is the absolute difference between the mean values of an input image $\mathbf{X}$ and output image $\mathbf{Y}$, i.e.,

$$AMBE\left(\mathbf{X},\mathbf{Y}\right)=\left|MB\left(\mathbf{X}\right)-MB\left(\mathbf{Y}\right)\right|, \tag{32}$$

where $MB\left(\mathbf{X}\right)$ and $MB\left(\mathbf{Y}\right)$ are the mean brightness values of $\mathbf{X}$ and $\mathbf{Y}$, respectively. The lower the value of *AMBE*, the better is the brightness preservation.

The discrete entropy *DE* of an image $\mathbf{X}$ measures its content, where a higher value indicates an image with richer details. It is defined as

$$DE\left(\mathbf{X}\right)=-\sum_{i=0}^{255}p\left(x_i\right)\log\left(p\left(x_i\right)\right), \tag{33}$$

where $p\left(x_i\right)$ is the probability of pixel intensity x_i which is estimated from the normalized histogram.

The edge based contrast measure *EBCM* is based on the observation that the human perception mechanisms are very sensitive to contours (or edges) [26]. The grey level corresponding to object frontiers is obtained by computing the average value of the pixel grey levels weighted by their edge values. The contrast $c\left(i,j\right)$ for a pixel of an image $\mathbf{X}$ located at $\left(i,j\right)$ is thus defined as

$$c\left(i,j\right)=\frac{\left|x\left(i,j\right)-e\left(i,j\right)\right|}{\left|x\left(i,j\right)+e\left(i,j\right)\right|},$$

where the mean edge grey level is

$$e\left(i,j\right)=\sum_{\left(k,l\right)\in\mathcal{N}\left(i,j\right)}g\left(k,l\right)x\left(k,l\right)\Big/\sum_{\left(k,l\right)\in\mathcal{N}\left(i,j\right)}g\left(k,l\right),$$

$\mathcal{N}\left(i,j\right)$ is the set of all neighbouring pixels of pixel $\left(i,j\right)$, and $g\left(k,l\right)$ is the edge value at pixel $\left(k,l\right)$. Without loss of generality we employ 3×3 neighbourhood, and $g\left(k,l\right)$ is computed using the magnitude of the gradient which is estimated from horizontal and vertical Sobel operators [1]. *EBCM* for image $\mathbf{X}$ is thus computed as the average contrast value, i.e.,

$$EBCM\left(\mathbf{X}\right)=\sum_{i=1}^{H}\sum_{j=1}^{W}c\left(i,j\right)\Big/H\times W. \tag{34}$$

It is expected that for an output image $\mathbf{Y}$ of an input image $\mathbf{X}$, the contrast is improved when $EBCM\left(\mathbf{Y}\right)\geq EBCM\left(\mathbf{X}\right)$.

A. Qualitative Assessment

1) Grey-Scale Images: Some contrast enhancement results on grey-scale images are shown in Fig. 3, Fig. 4, Fig. 5 and Fig. 6. The mapping functions used are shown in Fig. 7 (a)-(d), respectively.

The input image in Fig. 3 shows a firework display [21], and comprises very bright and dark objects. GHE has increased the overall brightness of the image, but the increase in contrast is not significant and the washout effect is apparent. Both the darker and brighter regions become even brighter. This is verified by the mapping function in Fig. 7(a) which maps input grey-level 0 to output grey-level 105. BPHEME and FHSABP preserve the input image average brightness value of 18. This results in the output image with very low brightness, and thus the contrast enhancement is not noticeable. The mapping function verifies this observation where the low output brightness and non-linear mapping from input to output are apparent. It is also clear from the mapping function that BPHEME performs almost one to one mapping when it is compared with the mapping function of FHSABP. This is due to the fact that BPHEME is designed to achieve brightness preservation as well as maximum

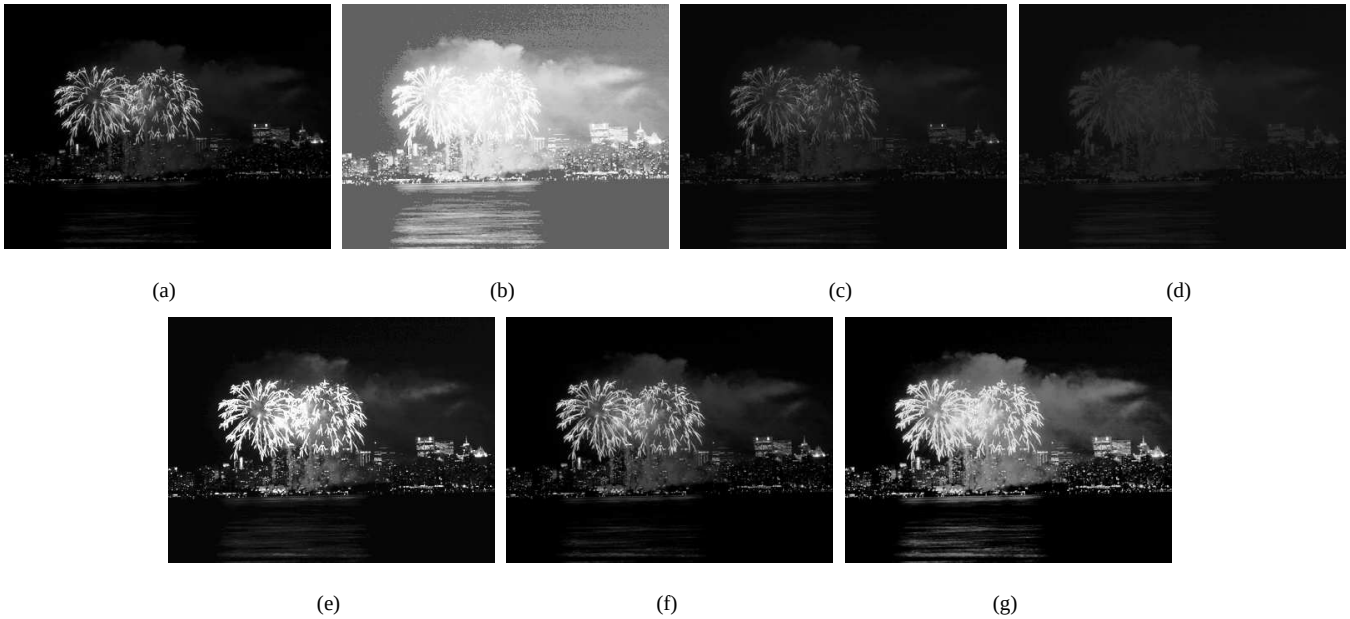

(a) (b) (c) (d)

(e) (f) (g)

Fig. 3. Contrast enhancement results for image *Fireworks*: (a) original image; (b) GHE; (c) BPHEME; (d) FHSABP; (e) HMF; (f) CEBGA; and (g) proposed.

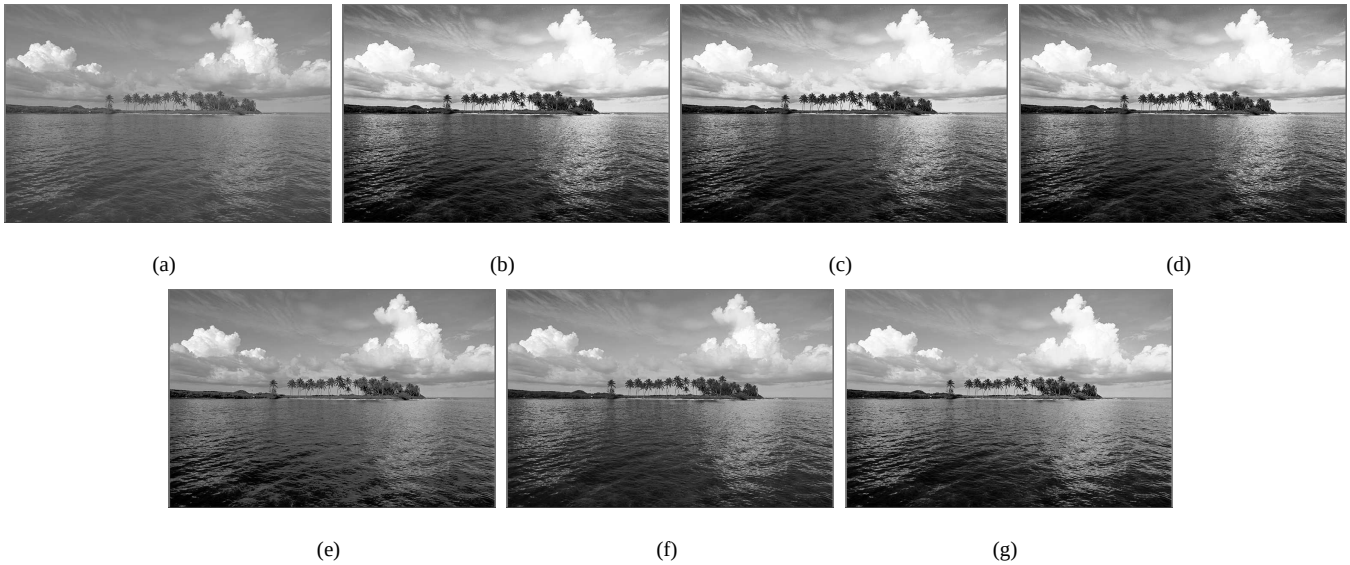

(a) (b) (c) (d)

(e) (f) (g)

Fig. 4. Contrast enhancement results for image *Island*: (a) original image; (b) GHE; (c) BPHEME; (d) FHSABP; (e) HMF; (f) CEBGA; and (g) proposed.

entropy. Thus, the mapping function of BPHEME achieves almost one-to-one mapping between input and output to guarantee the maximum entropy. The result of HMF is visually pleasing, providing high contrast as well as a high dynamic range. However, there are two different spark clusters due to the fireworks and the smoke between sparks. HMF over enhances the brighter pixels of the sparks and the surrounding smoke, so that the smoke pixels are also identified as spark pixels. This over enhancement is represented as a sharp change in the mapping function. Furthermore, due to over enhancement of the brighter pixels, the sparks due to the fireworks cannot be clearly differentiated. The over enhancement is due to forming a histogram from pixels with significant grey-level differences with their neighbours. The smoke around the sparks has similar but lower grey-level values. Thus, most of the smoke pixels cannot be differentiated from the spark pixels which results in mapping them to the same output grey-levels as that of the spark pixels. Due to the not sharp image details caused by the smoke from fireworks, CEBGA can only improve the overall brightness of the image. This is verified by the mapping function which

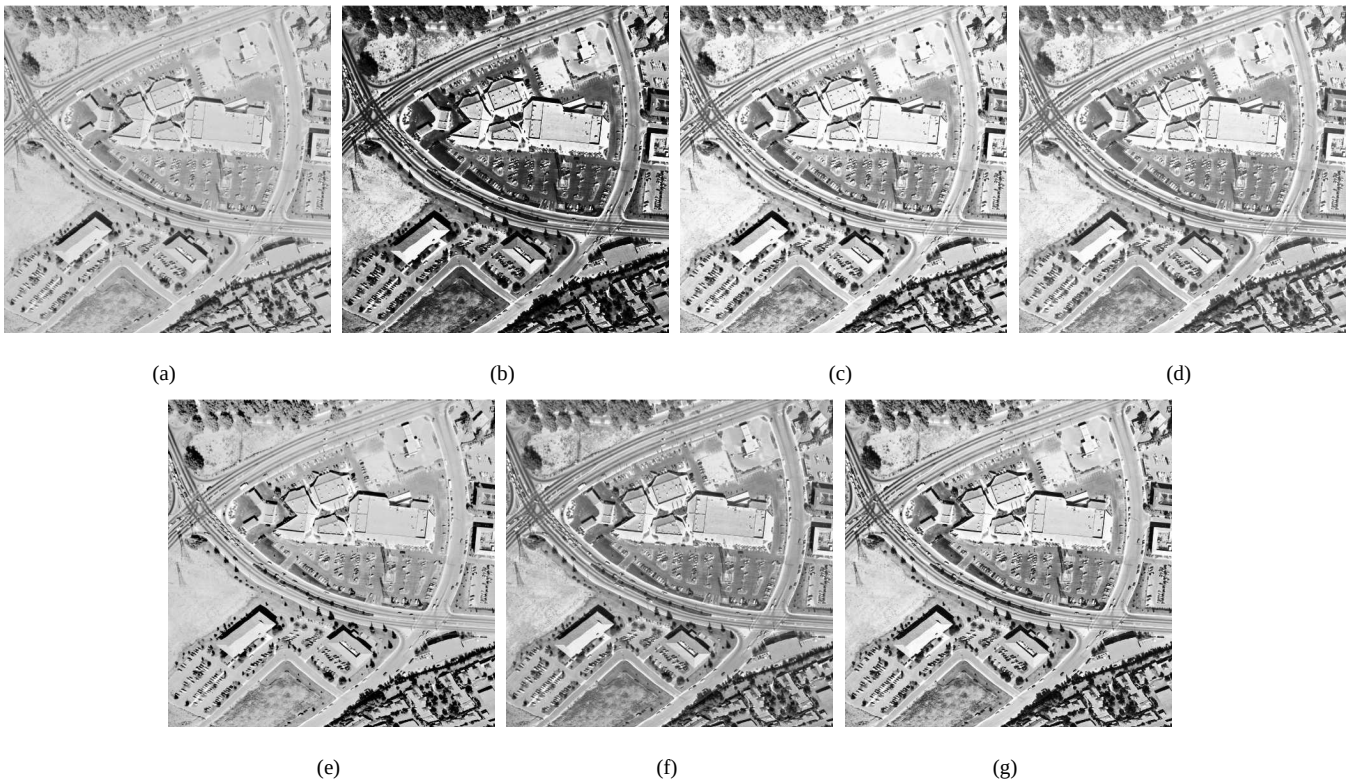

(a) (b) (c) (d)

(e) (f) (g)

Fig. 5. Contrast enhancement results for image *City*: (a) original image; (b) GHE; (c) BPHEME; (d) FHSABP; (e) HMF; (f) CEBGA; and (g) proposed.

(a) (b) (c) (d)

(e) (f) (g)

Fig. 6. Contrast enhancement results for image *Girl*: (a) original image; (b) GHE; (c) BPHEME; (d) FHSABP; (e) HMF; (f) CEBGA; and (g) proposed.

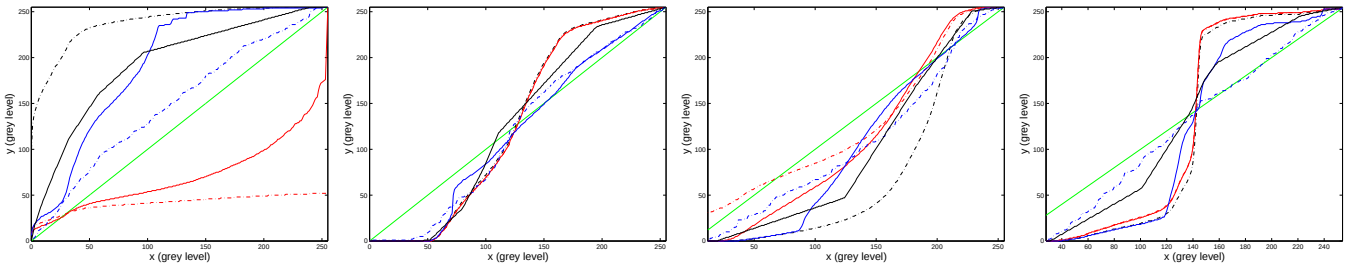

(a) (b) (c) (d)

Fig. 7. Mapping functions of enhanced images: (a) Fig. 3; (b) Fig. 4; (c) Fig. 5; and (d) Fig. 6. Key: Green solid line - no-change mapping; black dash-dotted line - GHE; red solid line - BPHEME; red dash-dotted line - FHSABP; blue solid line - HMF; blue dash-dotted line - CEBGA; and black solid line - proposed algorithm.

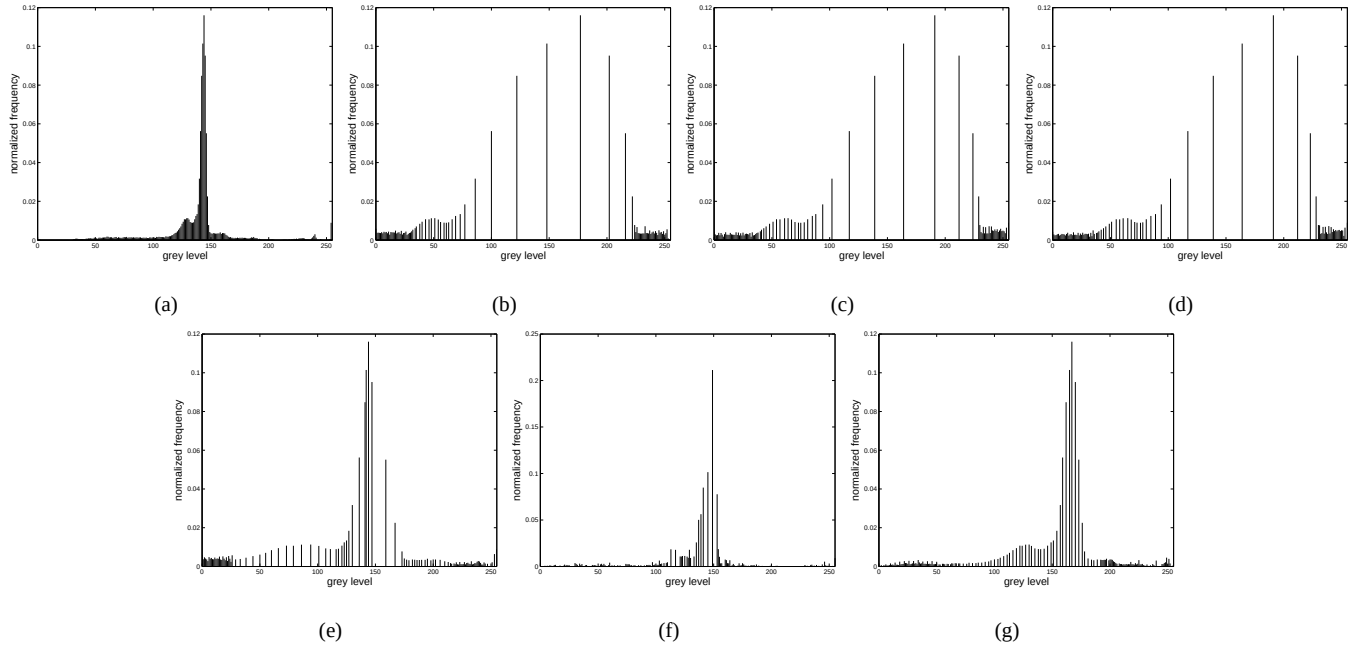

(a) (b) (c) (d)

(e) (f) (g)

Fig. 8. Histograms of original and enhanced images shown Fig. 6: (a) original image; (b) GHE; (c) BPHEME; (d) FHSABP; (e) HMF; (f) CEBGA; and (g) proposed.

is almost parallel to the no-change mapping. However, in the proposed algorithm, the dynamic range of the input image is modelled with GMM, which makes it possible to model the intensity values of sparks and smoke differently. Input grey-level values are assigned to output grey-level values according to their representative Gaussian components. The non-linear mapping is designed to utilise the full dynamic range of the output image. Thus, the proposed algorithm improves the overall contrast while preserving the details of the image.

The input image of an island in Fig. 4 [22] has average brightness value of 125. The results obtained by the different algorithms are similar as verified by the similar mapping functions in Fig. 7(b). BPHEME and FHSABP behaves exactly the same way as GHE when the average brightness value is 127.5 [13], [14]. Since the average brightness value of the input image is very close to 127.5, BPHEME and FHSABP algorithms obtains the similar target histograms. The slight difference of FHSABP from BPHEME is due to exact histogram specification used in FHSABP. The results of HMF and CEBGA are also a match because both algorithms employ similar edge information. Where the sky and sea converge, GHE, BPHEME and FHSABP provide a higher contrast than HMF and CEBGA. The proposed algorithm provides a contrast which is neither too high nor too low.

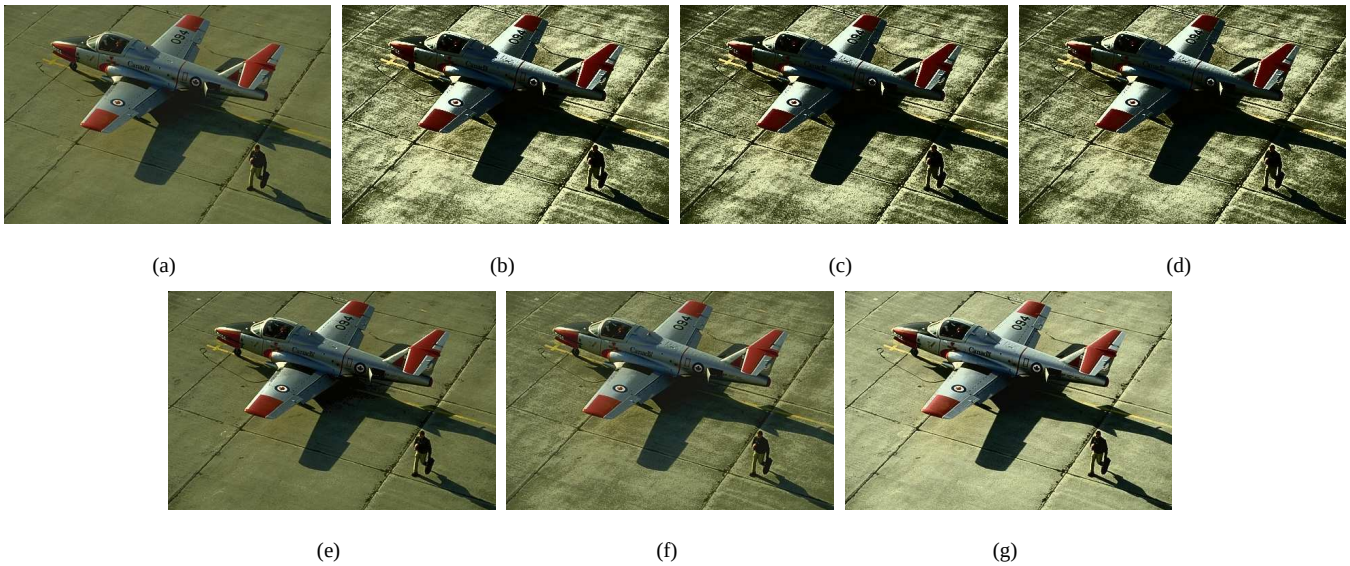

(a) (b) (c) (d)

(e) (f) (g)

Fig. 9. Contrast enhancement results for image *Plane*: (a) original image; (b) GHE; (c) BPHEME; (d) FHSABP; (e) HMF; (f) CEBGA; and (g) proposed.

The input image in Fig. 5 shows an aerial view of a junction in a city [23] with an average brightness value of 181 which is too high for recognizing the different objects. GHE increases the overall contrast of the image significantly, but the image looks darker as is verified by its mapping function in Fig. 7(c). The contrast improvements obtained by using BPHEME, FHSABP, HMF and CEBGA are very slight. HMF fails to provide an improvement due to weak edge information. The proposed algorithm, on the other hand, does not darken the image and produces sufficient contrast for the different objects to be recognized.

The image *Girl* shown in Fig. 6 consists of challenging conditions for an enhancement algorithm: very bright and dark objects, and average brightness value of 139 as can be verified from the histogram of the *Girl* image shown in Fig. 8(a). The histogram reveals that most of the grey levels of the input image are accumulated around grey level 144. Meanwhile, there are uniform grey level distributions on the left and right sides of the sharp peak in the middle. Because average brightness value of the input image is near to 127.5, GHE, BPHEME, and FHSABP performs very similar. This can be verified from the visual results, mapping functions shown Fig. 7(d), and histograms demonstrated in Fig. 8(b)-(d). As can be seen from the histograms, the output histograms fail to achieve smooth distribution between high and low values of grey levels. Thus, the enhancement results of GHE, BPHEME, and FHSABP are visually unpleasing. Meanwhile, the output histogram of HMF achieves smoother distribution in between low and high grey values, thus HMF achieves more natural looking output as shown in Fig. 8(e) when it is compared with that of GHE, BPHEME, and FHSABP. CEBGA produces natural looking output image, however the overall enhancement is not significant. As can be seen from mapping function and histogram in Fig. 7(d) and Fig. 8(f), CEBGA produces minor alterations on the input image. The result of the proposed algorithm is shown Fig. 6(g). The proposed algorithm preserves the overall distribution shape, meanwhile it achieves to redistribute the grey levels of the input image within the dynamic range without destroying natural look of the enhanced image. Although it slightly darkens the hair of woman, still the overall natural look is not destroyed while the perceived contrast is improved significantly.

2) Colour Images: In Fig. 9, the over enhancement provided by GHE, BPHEME and FHSABP whitens some areas of the concrete ground. HMF and CEBGA provide similar results where the slight contrast enhancement with respect to the input image is apparent, whereas the proposed algorithm enhances the contrast and the average brightness to improve the overall image quality. In Fig. 10, GHE, BPHEME, FHSABP and HMF cause part of the sky to be too bright. CEBGA and the

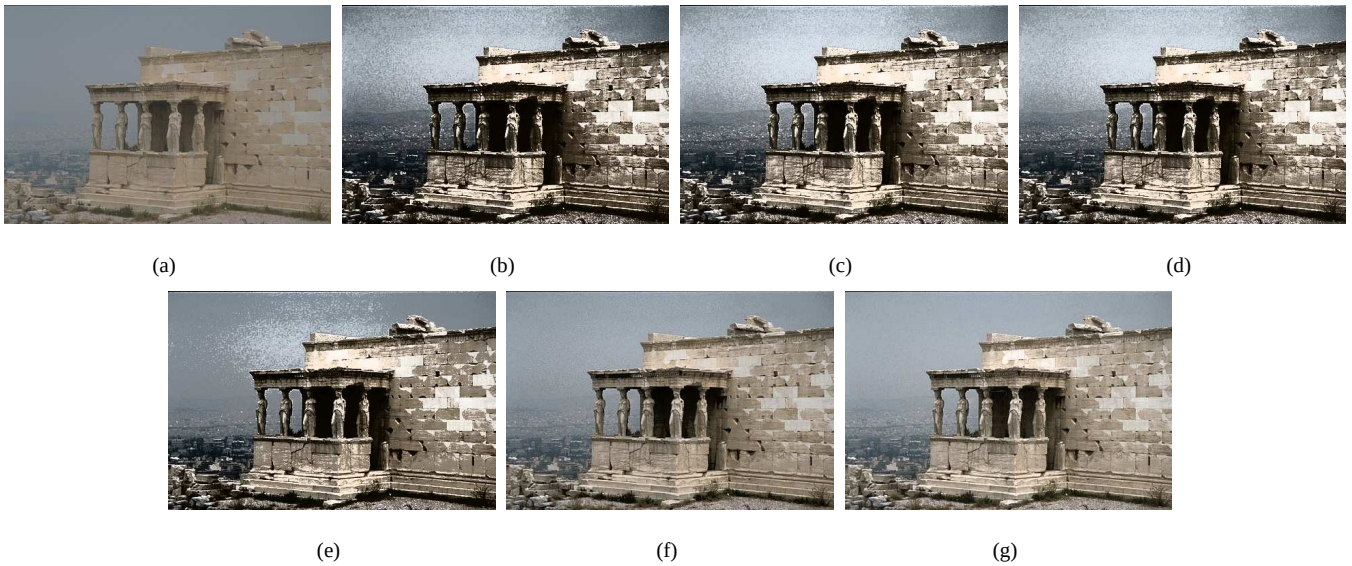

(a) (b) (c) (d)

(e) (f) (g)

Fig. 10. Contrast enhancement results for image *Ruins*: (a) original image; (b) GHE; (c) BPHEME; (d) FHSABP; (e) HMF; (f) CEBGA; and (g) proposed.

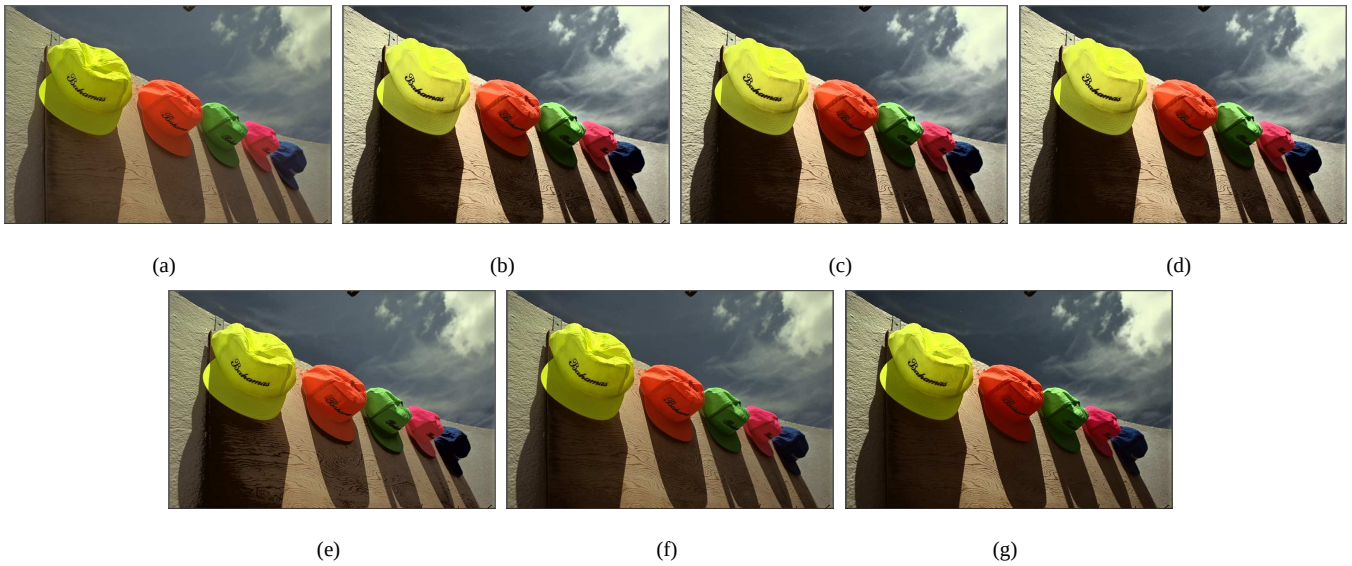

(a) (b) (c) (d)

(e) (f) (g)

Fig. 11. Contrast enhancement results for image *Hats*: (a) original image; (b) GHE; (c) BPHEME; (d) FHSABP; (e) HMF; (f) CEBGA; and (g) proposed.

proposed algorithm improve the overall contrast considerably and maintain high visual quality. In Fig. 11, GHE, BPHEME and FHSABP result in loss of details in the clouds and on the top of the yellow hat, whereas HMF and CEBGA retain the details while increasing the contrast. However, the contrast between the right side of the wall and the sky is not sufficiently high. The proposed algorithm keeps the details while improving the overall contrast. Finally, in Fig. 12, GHE makes the stones around the window and the pink flower very bright; hence, the enhanced image has an unnatural look. Although BPHEME and FHSABP performs better than GHE, it still does not remove this effect completely. This effect is reduced by HMF, CEBGA and the proposed algorithm. Also, the colours of window and wall are better differentiated in the result of the proposed algorithm.

Turgay: Please skip this paragraph as it needs new evaluation scores. *In order to assign a visual assessment score to each algorithm for each enhanced image, subjective perceived quality tests are performed by a group of ten subjects on the results of the five algorithms for the eight test images. For each test on a test image, a subject is shown two images: the test image and the image processed by one of the five algorithms. The subject is then asked to score the quality of the processed image*

(a) (b) (c) (d)

(e) (f) (g)

Fig. 12. Contrast enhancement results for image *Window*: (a) original image; (b) GHE; (c) BPHEME; (d) FHSABP; (e) HMF; (f) CEBGA; and (g) proposed.

TABLE II

AVERAGE OF SUBJECTIVE QUALITY TEST SCORES.

Image	GHE	FHSABP	HMF	CEBGA	Prop.
Fireworks	“Bad”	“Bad”	“Good”	“Good”	“Good”
Island	“Bad”	“Bad”	“Good”	“Good”	“Good”
City	“Good”	“Bad”	“Bad”	“Bad”	“Good”
Wolf	“Bad”	“Bad”	“Bad”	“Good”	“Good”
Plane	“Bad”	“Bad”	“Good”	“Good”	“Good”
Ruins	“Bad”	“Bad”	“Bad”	“Good”	“Good”
Hats	“Good”	“Good”	“Bad”	“Good”	“Good”
Window	“Good”	“Good”	“Bad”	“Bad”	“Good”

by assigning a fuzzy score of “Bad” for weak enhancement, and “Good” for visually pleasing enhancement. The test on the same input image is repeated for the processed images generated by the other four algorithms. For each processed image of an algorithm, we average the scores from the ten subjects. In the averaging operation, when the number of “Good” scores are higher than “Bad” scores, then the processed image is deemed as “Good”, and vice versa. The visual assessment scores as shown in Table II validate our subjective evaluations that the proposed algorithm provides good visual quality enhancement.

B. Quantitative Assessment

The quantitative measures *AMBE*, *DE*, and *EBCM* may fail to provide enhancement measures which are parallel with perceived image quality. For instance for *Girl* image, GHE, BPHEME, FHSABP, HMF, CEBGA, and proposed method produces *AMBE* values of 5.60, 5.50, 5.50, 10.30, 1.60, and 12.90, respectively. CEBGA achieves the best in terms of brightness preservation where the proposed method performs the worst. The *Girl* image has *DE* value of 3.87, meanwhile GHE, BPHEME, FHSABP, HMF, CEBGA, and proposed method produces *DE* values of 3.65, 3.65, 3.65, 3.70, 3.45, and 3.81, respectively. The proposed method achieves the best *DE* value. The *Girl* image has very low contrast measure *EBCM* value of 0.08. GHE, BPHEME, FHSABP, HMF, CEBGA, and proposed method results in *EBCM* values of 0.23, 0.22, 0.22, 0.17, 0.11, and 0.12. All methods achieve to produce higher values of *EBCM* with respect to the *EBCM* value of original *Girl* image. GHE, BPHEME, and FHSABP produces the highest values of *EBCM*, however perceived visual quality is not natural. Although there is a

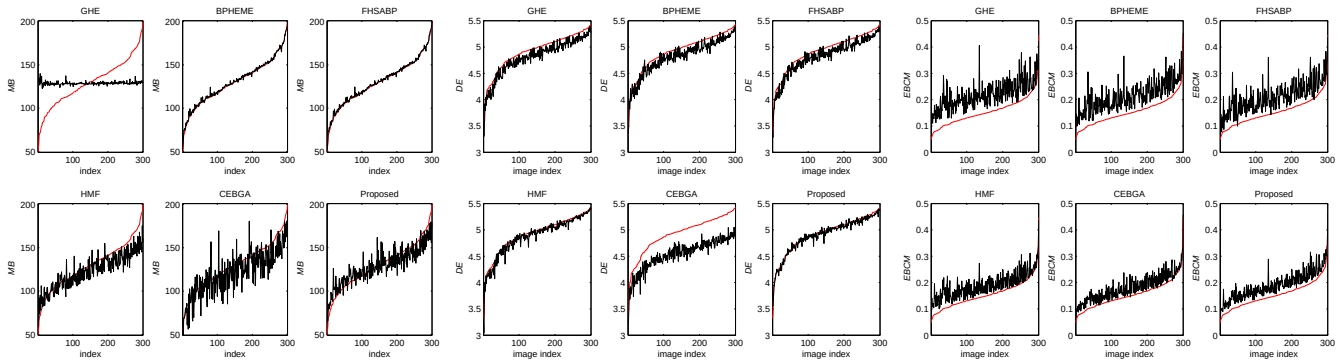

(a) (b) (c)

Fig. 13. Quantitative performance results on 300 images from Berkeley dataset [24]: (a) results for *MB*; (b) results for *DE*; and (c) results for *EBCM*. The reference measurements from the original image is shown in red colour, meanwhile the measurements from the processed images resulted from different algorithms are shown in black colour.

correlation between between *EBCM* and perceived contrast enhancement, it does not always mean that the higher value of *EBCM* means better perceived contrast enhancement.

In order to test algorithms' performance quantitatively in terms of brightness and entropy preservation as well as contrast improvement, they are applied on 300 test images of Berkeley image dataset [24]. *MB*, *DE*, and *EBCM* values are computed from original and processed images. In reported results, the measurement values from the original images are sorted in ascending order and the images are indexed accordingly. The quantitative results for *MB*, *DE*, and *EBCM* are shown in Fig. 13(a), (b), and (c), respectively.

The *MB* values in Fig. 13(a) show that except GHE all algorithms follow general trend in the mean brightness value, *i.e.*when the mean brightness value of the original image is low so do the output image, and vice versa. GHE consistently maps the mean brightness value of the output image very close to 127.5 which is the mid value of the 8-bit grey-level dynamic range. The average of *AMBE* resulted from GHE over dataset is 21.09. Meanwhile, BPHEME and FHSABP achieves the best brightness preservation as can be seen from the plots. Both algorithms produces very similar results for the whole dataset. This is mainly due to the target histograms of BPHEME and FHSABP are similar to each other. The averages of *AMBE* resulted from BPHEME and FHSABP over dataset are 1.30 and 1.28, respectively. On the average, the proposed method performs better than HMF and HMF performs better than CEBGA in terms of brightness preservation. The averages of *AMBE* resulted from HMF, CEBGA, and the proposed method are 10.07, 12.23, and 8.80, respectively.

GHE, BPHEME, and FHSABP performs very similar results in terms of *DE* on Berkeley dataset as shown Fig. 13(b). The average absolute discrete entropy difference between the input and out images over dataset for GHE, BPHEME, and FHSABP are 0.12, 0.12, and 0.11, respectively. Fig. 13(b) also shows that CEBGA performs the worst with the average absolute discrete entropy difference of 0.38. Meanwhile, HMF and the proposed method achieves good performance in terms of entropy. The average absolute discrete entropy difference between the input and out images over dataset for HMF and the proposed method are 0.05, and 0.04, respectively. Since the entropy is related with the overall image content, one can say that for Berkeley dataset the proposed method can preserve the overall content of the image while improving its contrast.

The *EBCM* measures are shown in Fig. 13(c). Although high *EBCM* does not always mean a good and natural image enhancement, however it is, at least, expected that the output image's *EBCM* value is higher than that of the input image. Out of 300 images in the dataset, GHE, BPHEME, FHSABP, HMF, CEBGA, and proposed method produces 294, 300, 296, 293,

(a) (b) (c)

Fig. 14. High dynamic range compression results. (a) Original image. Processed image obtained using: (b) [27]; and (c) proposed algorithm.

286, and 300 output images, respectively, which have higher than or equal to *EBCM* values with that of the input images. Meanwhile, the average absolute *EBCM* difference between the input and out images over dataset for GHE, BPHEME, FHSABP, HMF, CEBGA, and proposed method are 0.0652, 0.0603, 0.0573, 0.0361, 0.0278, and 0.0366, respectively. As expected, GHE provides the highest contrast improvement in terms of *EBCM*. Meanwhile, BPHEME and FHSABP performs very similar and slightly worse than GHE. BPHEME performs better than FHSABP, because of lowpass filtering employed in exact histogram specification used in FHSABP. Meanwhile, the proposed method and HMF performs similar and CEBGA provides the worst performance. It is worth to note that only two algorithms, BPHEME and the proposed method, achieves to make *EBCM* improvement with respect to the input image.

C. Application to High Dynamic Range Compression

The proposed algorithm can be applied for rendering high dynamic range (HDR) images on conventional displays. Thus, we compare some of our results with those of the state-of-the-art method proposed by Fattal et al. [27]. In the Fattal et al. method, the gradient field of the luminance image is manipulated by attenuating the magnitudes of large gradients. A low dynamic range image is then obtained by solving a Poisson equation on the modified gradient field. The results in [27], a few of which are in Fig. 14, show that the method is capable of drastic dynamic range compression, while preserving fine details and avoiding common artefacts such as halos, gradient reversals, or loss of local contrast. Fig. 14 also shows that the proposed algorithm produces comparable results. It is worth noting that our results are obtained without any parameter tuning.

IV. Conclusions

In this paper, we proposed an automatic image enhancement algorithm which employs Gaussian mixture modelling of an input image to perform non-linear data mapping for generating visually pleasing enhancement on different types of images. Performance comparisons with state-of-the-art techniques show that the proposed algorithm can achieve good enough image equalization even under diverse illumination conditions. The proposed algorithm can be applied to both grey-level and colour

images without any parameter tuning. It can also be used to render high dynamic range images. It does not distract the overall content of an input image with high enough contrast. It further improves the colour content, brightness and contrast of an image automatically.

REFERENCES

[1] R. C. Gonzalez and R. E. Woods, *Digital Image Processing*, 3rd ed. Upper Saddle River, NJ, USA: Prentice-Hall, Inc., 2006.

[2] D. Jobson, Z. Rahman, and G. Woodell, "A multiscale retinex for bridging the gap between color images and the human observation of scenes," *IEEE Trans. Image Process.*, vol. 6, no. 7, pp. 965–976, Jul 1997.

[3] J. Mukherjee and S. Mitra, "Enhancement of color images by scaling the dct coefficients," *IEEE Trans. Image Process.*, vol. 17, no. 10, pp. 1783–1794, Oct 2008.

[4] S. Agaian, B. Silver, and K. Panetta, "Transform coefficient histogram-based image enhancement algorithms using contrast entropy," *IEEE Trans. Image Process.*, vol. 16, no. 3, pp. 741–758, Mar 2007.

[5] R. Dale-Jones and T. Tjahjadi, "A study and modification of the local histogram equalization algorithm," *Pattern Recognit.*, vol. 26, no. 9, pp. 1373–1381, September 1993.

[6] T. K. Kim, J. K. Paik, and B. S. Kang, "Contrast enhancement system using spatially adaptive histogram equalization with temporal filtering," *IEEE Trans. Consumer Electron.*, vol. 44, no. 1, pp. 82–87, Feb 1998.

[7] C.-C. Sun, S.-J. Ruan, M.-C. Shie, and T.-W. Pai, "Dynamic contrast enhancement based on histogram specification," *IEEE Trans. Consumer Electron.*, vol. 51, no. 4, pp. 1300–1305, Nov 2005.

[8] Y.-T. Kim, "Contrast enhancement using brightness preserving bi-histogram equalization," *IEEE Trans. Consumer Electron.*, vol. 43, no. 1, pp. 1–8, Feb 1997.

[9] Y. Wang, Q. Chen, and B. Zhang, "Image enhancement based on equal area dualistic sub-image histogram equalization method," *IEEE Trans. Consumer Electron.*, vol. 45, no. 1, pp. 68–75, Feb 1999.

[10] S.-D. Chen and A. Ramli, "Minimum mean brightness error bi-histogram equalization in contrast enhancement," *IEEE Trans. Consumer Electron.*, vol. 49, no. 4, pp. 1310–1319, Nov 2003.

[11] ——, "Contrast enhancement using recursive mean-separate histogram equalization for scalable brightness preservation," *IEEE Trans. Consumer Electron.*, vol. 49, no. 4, pp. 1301–1309, Nov 2003.

[12] M. Abdullah-Al-Wadud, M. Kabir, M. Dewan, and O. Chae, "A Dynamic Histogram Equalization for Image Contrast Enhancement," *IEEE Trans. Consumer Electron.*, vol. 53, no. 2, pp. 593–600, May 2007.

[13] C. Wang and Z. Ye, "Brightness preserving histogram equalization with maximum entropy: a variational perspective," *IEEE Trans. Consumer Electron.*, vol. 51, no. 4, Nov 2005.

[14] C. Wang, J. Peng, and Z. Ye, "Flattest histogram specification with accurate brightness preservation," *IET Image Process.*, vol. 2, no. 5, pp. 249–262, Oct 2008.

[15] T. Arici, S. Dikbas, and Y. Altunbasak, "A Histogram Modification Framework and Its Application for Image Contrast Enhancement," *IEEE Trans. Image Process.*, vol. 18, no. 9, pp. 1921–1935, Sep 2009.

[16] S. Hashemi, S. Kiani, N. Noroozi, and M. E. Moghaddam, "An image contrast enhancement method based on genetic algorithm," *Pattern Recognit. Lett.*, vol. 31, no. 13, pp. 1816–1824, 2010.

[17] D. Reynolds and R. Rose, "Robust text-independent speaker identification using gaussian mixture speaker models," *IEEE Trans. Speech Audio Process.*, vol. 3, no. 1, pp. 72–83, Jan 1995.

[18] R. O. Duda, P. E. Hart, and D. G. Stork, *Pattern Classification*, 2nd ed. Wiley-Interscience, Nov 2000.

[19] M. Figueiredo and A. Jain, "Unsupervised learning of finite mixture models," *IEEE Trans. Pattern Anal. Mach. Intell.*, vol. 24, no. 3, pp. 381–396, Mar 2002.

[20] M. Abramowitz and I. A. Stegun, *Handbook of Mathematical Functions with Formulas, Graphs, and Mathematical Tables*. New York: Dover Publications, 1965.

[21] Retrieved on Aug 2010 from the World Wide Web: http://www.imagecompression.info/test_images/.

[22] Retrieved on Aug 2010 from the World Wide Web: http://r0k.us/graphics/kodak/.

[23] Retrieved on Aug 2010 from the World Wide Web: http://sipi.usc.edu/database/.

[24] D. Martin, C. Fowlkes, D. Tal, and J. Malik, "A database of human segmented natural images and its application to evaluating segmentation algorithms and measuring ecological statistics," in *Proc. 8th Int. Conf. Comput. Vis.*, vol. 2, Jul 2001, pp. 416–423.

[25] C. E. Shannon, "A mathematical theory of communication," *Bell Syst. Tech. J.*, vol. 27, 1948.

[26] A. Beghdadi and A. L. Negrate, “Contrast enhancement technique based on local detection of edges,” *Comput. Vis. Graph. Image Process.*, vol. 46, no. 2, pp. 162–174, 1989.

[27] R. Fattal, D. Lischinski, and M. Werman, “Gradient domain high dynamic range compression,” in *Proc. 29th Annual Conf. Comput. Graph. Interactive Techniques*. New York, NY, USA: ACM, 2002, pp. 249–256.